AIP Journal of Applied Physics

X-ray diffraction analysis of concentration and residual stress gradients in nitrogen-implanted niobium and molybdenum

Satish I. Rao, Baoping He, C. R. Houska, and K. Grabowski

Citation: Journal of Applied Physics **69**, 8111 (1991); doi: 10.1063/1.347461
View online: http://dx.doi.org/10.1063/1.347461
View Table of Contents: http://scitation.aip.org/content/aip/journal/jap/69/12?ver=pdfcov
Published by the AIP Publishing

Articles you may be interested in
Characteristics of a molybdenum X-pinch X-ray source as a probe source for X-ray diffraction studies
Rev. Sci. Instrum. **86**, 033507 (2015); 10.1063/1.4915496

Anisotropic strain-stress state and intermixing in epitaxial Mo(110)/Ni(111) multilayers: An x-ray diffraction study
J. Appl. Phys. **107**, 023515 (2010); 10.1063/1.3284079

X-ray diffraction measurements of Mo melting to 119 GPa and the high pressure phase diagram
J. Chem. Phys. **130**, 124509 (2009); 10.1063/1.3082030

High-efficiency diffractive x-ray optics from sectioned multilayers
Appl. Phys. Lett. **86**, 151109 (2005); 10.1063/1.1897061

Structural characterization of a Mo/Si multilayer reflector by means of x-ray diffraction measurements
J. Vac. Sci. Technol. A **15**, 2291 (1997); 10.1116/1.580737

MIT LINCOLN LABORATORY CAREERS
Discover the satisfaction of innovation and service to the nation
- Space Control
- Air & Missile Defense
- Communications Systems & Cyber Security
- Intelligence, Surveillance and Reconnaissance Systems
- Advanced Electronics
- Tactical Systems
- Homeland Protection
- Air Traffic Control

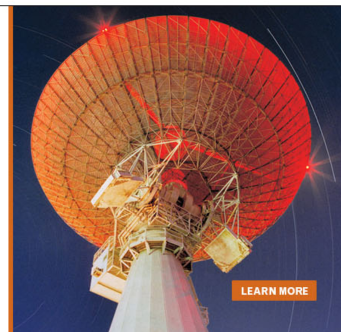

[This article is copyrighted as indicated in the article. Reuse of AIP content is subject to the terms at: http://scitation.aip.org/termsconditions. Downloaded to] IP: 128.173.126.47 On: Wed, 06 May 2015 20:47:48

X-ray diffraction analysis of concentration and residual stress gradients in nitrogen-implanted niobium and molybdenum

Satish I. Rao, Baoping He, and C. R. Houska
Department of Materials Engineering, Virginia Polytechnic Institute and State University, Blacksburg, Virginia 24061

K. Grabowski
Naval Research Laboratory, Washington, DC 20375

(Received 15 December 1989; accepted for publication 15 February 1991)

Large biaxial residual strains are developed after a 5-at.% implantation of N into Nb and Mo. The results indicate that the dominant source of internal strain arises from N located in interstitial sites. For Nb implanted at liquid-nitrogen temperature, the N atoms are located in octahedral sites. However, the data allow for some clustering as di- or tri-interstitials at the highest concentration (~5 at. % N). Radiation damage is present as small vacancy and interstitial loops. Since vacancies and self-interstitials are present in nearly equal concentrations, the overall bulk dilatation cancels. However, because of their small size, a lesser core expansion has been included as a correction to the overall residual strain. Although one can obtain an estimate of the N distribution from TRIM, a more accurate description must include the distribution of knock-on energy. The latter has an important influence on the redistribution of N relative to that predicted by TRIM. Both host lattices (Nb and Mo) behave like "rigid containers" in directions parallel to the free surface and give a magnified elastic response normal to the free surface.

I. INTRODUCTION

Ion implantation of N atoms into single crystals of Mo, Nb introduces composition gradients near the surface. The nitrogen atoms are known to dissolve interstitially in the bcc Nb lattice at the octahedral interstitial positions.[1] This results in a volume expansion of the bcc lattice that maintains the cubic symmetry if all types of octahedral positions are occupied equally. The expansion is linearly proportional to the concentration of N.[2,3] Lattice damage from knock-on defects introduces a correction due to the core regions of interstitial and vacancy loops. The presence of nearly equal numbers of interstitials and vacancies essentially cancels the overall volume change produced by loop defects. Three-dimensional clusters of interstitials and vacancies need not produce a cancellation.

The lattice parameter or d spacing profile associated with implanted N and knock-on lattice damage results in asymmetrically broadened diffraction profiles.[4] Line-shape analysis has been used to extract composition versus depth curves for diffused films.[5,6] For ion-implanted zones containing interstitial atoms, one must allow for the effect of static displacement fields about the interstitial implants as well as for damage related defects in the intensity calculations.

Volume changes resulting from ion implantation produces a biaxial residual stress profile due to the constraint imposed by the underlying material or substrate.[7,8] Such internal elastic stresses may be relieved by the formation of dislocation arrays[9,10] and other mechanisms. The relative change in d spacing at a given depth z below the free surface is equal to the sum of the free expansion strain $\epsilon_f(z)$ due to the defects and the related elastic strain $\epsilon_e(z)$.[7,8] If the elastic strains are completely relieved, then the relative change in d spacing is identically equal to the free expansion strain. The latter case was found for thick diffused films.[5] Methods of separating the two strains has been discussed in a previous paper.[7] Large residual strain gradients can develop along ion-implanted zones that must be accounted for in the analysis of diffraction profiles.

To illustrate these methods, we examine Bragg profiles from a 2500-Å (111)Nb film, a 6000-Å (100) Nb film, as well as profiles from bulk Mo single crystals all implanted with N to an average concentration of 5 at. % at liquid-nitrogen temperature (LNT). A Mo crystal was also implanted at room temperature (RT) under otherwise identical conditions. Four different implantation energies produce a nonuniform and overlapping N distribution when superimposed. Variations in composition produced related variations in d spacing and Bragg peaks become broadened into intensity bands.

II. ANALYSIS OF EXPERIMENTAL RESULTS

Nb single-crystal films were deposited onto sapphire substrates at 850 °C with a vacuum better than 10^{-10} Torr at the Naval Research Laboratory, Washington, DC. Two were deposited onto (001) sapphire substrates with a thickness of 2500 Å, and a (111) orientation. A third film was deposited onto a (012)-oriented sapphire substrate with a thickness of 6000 Å, and a (100) orientation. Two of the films having (111) and (100) orientations were implanted with N at LNT to an average level of 5 at. % (samples S1 and S3 for future reference). The four implantation energies and fluences, introduced with decreasing energy, are given in Table I. One of the (111)-oriented films was used as an unimplanted standard (S2). In addition, to the Nb films, two electropolished (111)-oriented

 0021-8979/91/128111-08$03.00 © 1991 American Institute of Physics

[This article is copyrighted as indicated in the article. Reuse of AIP content is subject to the terms at: http://scitation.aip.org/termsconditions. Downloaded to] IP: 128.173.126.47 On: Wed, 06 May 2015 20:47:48

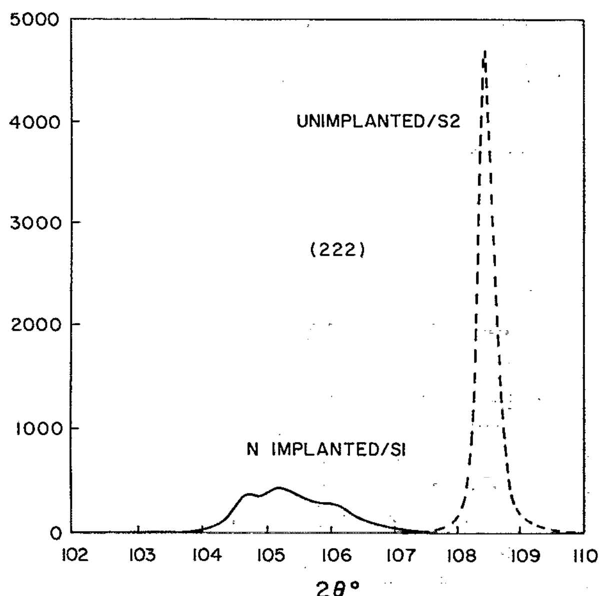

FIG. 1. X-ray diffraction profiles from implanted (5 at. % N) and unimplanted Nb [2500 Å, (110)] single-crystal films using Cu$K\alpha$l radiation.

TABLE I. Energy, range, standard deviation (straggling) and fluences of the four implantations used for Mo single crystals and Nb single-crystal films.

Energy (kv)	Range (Å)	Standard Deviation (Å)	Fluence (atoms/Å^2)
190	2094	729	4.92
89	1076	463	2.00
43	559	275	1.19
17.5	259	141	0.552

Mo single crystals were implanted with N in the same way. One of them was at LNT (C1), and the other one at RT (C2).

All samples were examined using monochromatic Cu$K\alpha$l radiation from a fine focus tube and a Siemens ω-drive diffractometer. At least two Bragg diffraction profiles (intensity bands) from each of the samples were examined. The (222) diffraction profiles from samples S1 and S2 are shown in Fig. 1. Typically, the intensity profile from an implanted film is broadened asymmetrically toward a lower 2θ value as a result of larger nonuniform d spacings. The intensity band from the implanted films can also show a fine structure [Figs. 1 and 2(a)] relative to the single peak from unimplanted pure Nb. Since this Nb film is only 2500 Å thick, no pure Nb remains.

Figures 2(c) and 2(d) show the (222) diffraction profiles from samples C1 and C2, respectively. In these cases, the diffraction profiles show a broad low-intensity peak without fine structure at the low-angle region corresponding to the scattering from the thin implanted zone. The intense peak at the higher angles is scattering from the Mo single-crystal substrate. For these samples, the region between the two peaks also shows a measurable scattering. The separation between the peaks as well as the broadening of the low-angle peak is somewhat greater for the Mo crystal implanted at RT (C2), as compared to sample C1, implanted at LNT. Figure 2(b) shows the (400) intensity band from the 6000-Å Nb film (S3) implanted at LNT. The scattering curve is similar to the ones from the implanted Mo single crystals but the area of the peak corresponding to the unimplanted regions is smaller. Additional intensity bands from planes inclined to the surface by ~35° were obtained from each of the samples (see Fig. 3). Rocking curves scanning perpendicular to the radial direction were obtained from each of the reflections at five 2θ values

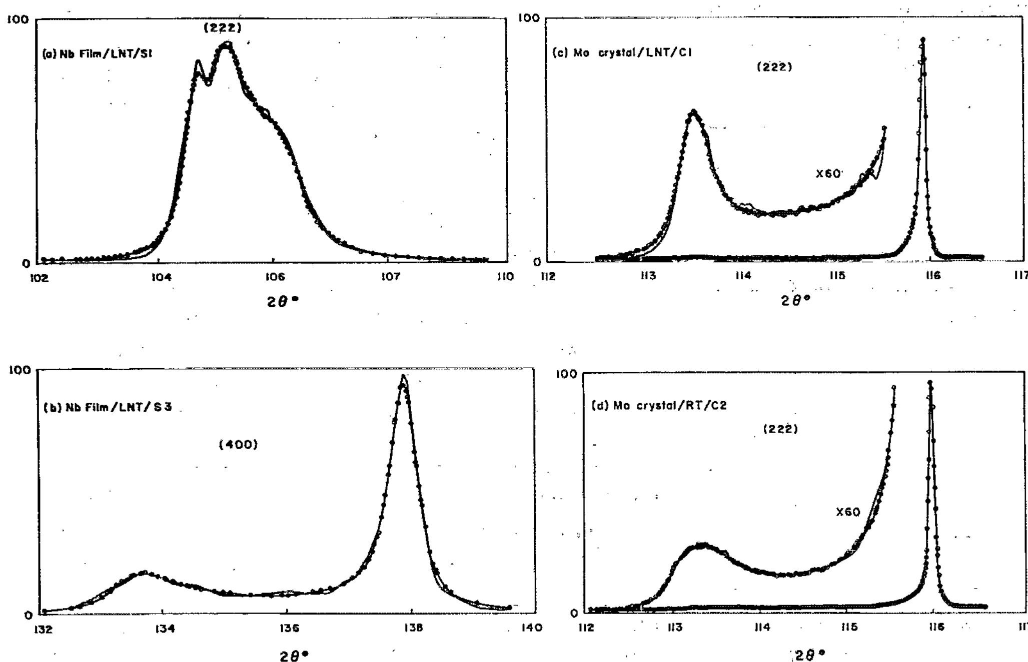

FIG. 2. Intensity bands from 5-at. % N samples: (a) Nb, 2500 Å, (111) film implanted at LNT; (b) Nb, 6000-Å, (100) films implanted at LNT; (c) Mo single crystal implanted at LNT; (d) Mo single crystal implanted at RT. All were obtained using Cu$K\alpha$l. In each case, the points are determined by experiment and the solid curves are simulated using d spacing profiles shown in Figs. 5 and 7.

[This article is copyrighted as indicated in the article. Reuse of AIP content is subject to the terms at: http://scitation.aip.org/termsconditions. Downloaded to] IP: 128.173.126.47 On: Wed, 06 May 2015 20:47:48

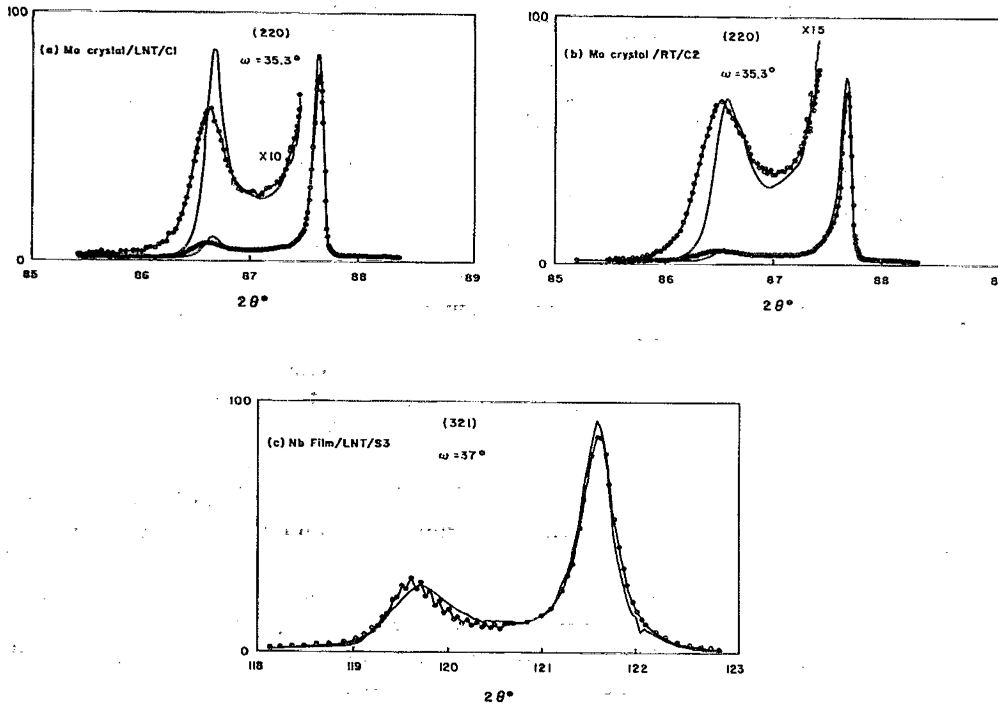

FIG. 3. Intensity bands from samples shown in Fig. 2 but tilted as indicated. Points are determined from experiment and solid curves are simulated from Figs. 5 and 7 using a purely elastic model.

from samples S3, C1, and C2., (Fig. 4). The five radial points chosen were: (i) the maximum positions, (ii) 2θ positions at which the intensity is half of the maximum intensity of the small peak on both low- and high-angle sides, and (iii) 2θ position halfway between the maxima.

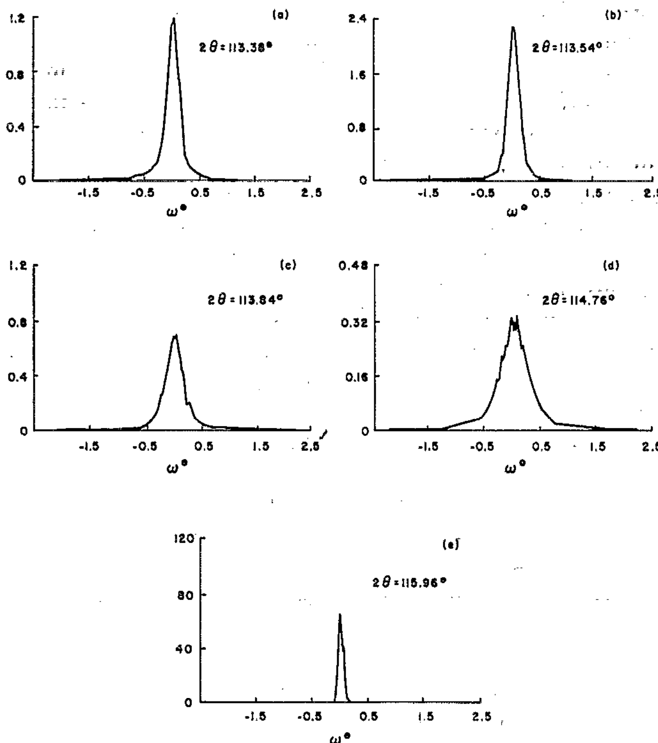

FIG. 4. Typical rocking curves obtained at indicated 2θ values which may be associated with selected points shown in Fig. 2(c) for Mo.

Initially, TRIM (Ref. 11) was used to simulate the distribution of implanted N from the data given in Table I. The fractional change in the average volume of the Nb unit cell, per unit concentration of N, $(1/V)(\partial V/\partial C)$, was obtained from available experimental data[1,3] and is equal to 0.385. No experimental data are available in the literature for N in Mo. We find a value of 0.44 after a fitting of the intensity band data from Mo crystals implanted with N. This is in reasonable agreement with the theoretical calculations based on structure data.[12] Free expansion strain profiles for Nb films and Mo crystals are shown in Figs. 5(a) and 5(b).

The strain variation with depth is magnified in terms of the free expansion strain by a factor β^{el} due to the rigid substrate. This is

$$\beta^{el} = (C_{11} + 2C_{12})/(C_{11} + C_{an}^{\Omega}), \qquad (1)$$

where $C_{an} = C_{44} - \frac{1}{2}(C_{11} - C_{12})$; C_{11}, C_{12} and C_{44} are the cubic elastic constants of the implanted zone;

$$\Omega = 4(\alpha_3^2\beta_3^2 + \alpha_3^2\gamma_3^2 + \beta_3^2\gamma_3^2),$$

and α_3, β_3, and γ_3 are direction cosines of the normal to the free surface (x_3 direction) with respect to the cubic coordinate system. The elastic strain profile is directly proportional to the variation of C and the total strain at any tilt angle ω is[7]

$$\epsilon'_{\omega}(x_3) = \frac{C(x_3)}{3V}\frac{\partial V}{\partial C}\beta^{el}\cos^2\omega. \qquad (2)$$

$\epsilon'_{\omega}(x_3)$ goes to zero linearly at $\omega = 90°$ with a $\cos^2\omega$ dependence. Equation (2) takes into account the elastic constraint due to the substrate. Elastic constants of Nb and Mo are listed in Table II. The (222) and (400) diffraction

[This article is copyrighted as indicated in the article. Reuse of AIP content is subject to the terms at: http://scitation.aip.org/termsconditions. Downloaded to] IP: 128.173.126.47 On: Wed, 06 May 2015 20:47:48

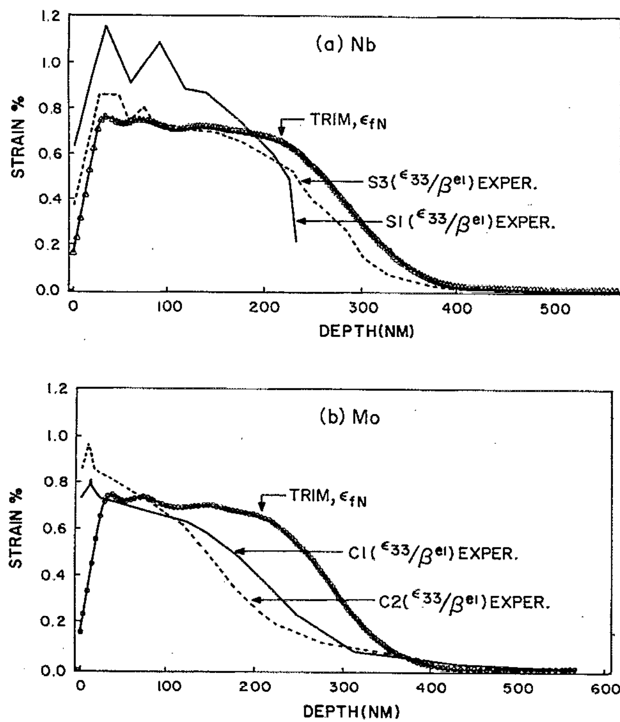

FIG. 5. Free expansion strain profiles for (a) Nb, 2500-Å, (111) film (S1); Nb, 6000-Å, (100) film (S3). (b) Mo (100) single crystals implanted at LNT (C1) and RT (C2). TRIM is also shown in each case.

profiles from samples S1 and S3, respectively, and the (222) diffraction profile from samples C1 and C2, were simulated by using the magnified strain profile and the basic intensity equation, given by Eq. (1) of Ref. 4, with absorption included.

If the implanted zone is completely constrained by the underlying substrate, then the displacement components along the a_1 and a_2 directions (directions parallel to the free surface) X_m and Y_m, are zero since $\epsilon'_{11}(x_3) = \epsilon'_{22}(x_3) = 0$, at each position x_3. Also, the strains normal to the free surface ϵ_{33}, are only a function of x_3. By introducing these simplifications into the basic diffraction equations, and summing over all layers in the implanted zone (model 1, Ref. 4),

TABLE II. Elastic constants of Nb and Mo.[a]

Elastic Constants (GPA)	Nb	Mo
C_{11}	245.6	469.6
C_{12}	138.7	167.6
C_{44}	29.3	106.8
$C_{an}^{(7)}$	24.2	-44.4
Ratios[b]		
A_{111}	-1.45	-0.96
$\beta_{el}^{111} = 1 - A_{111}$	2.45	1.96
A_{100}	-1.19	-0.71
$\beta_{el}^{100} = 1 - A_{100}$	2.13	1.71

[a]See Ref. 13.
[b]See Ref. 7.

$$I = K'F^2 \frac{\sin^2 \pi N_1 h'_1}{(\pi N_1 h'_1)^2} \frac{\sin^2 \pi N_2 h'_2}{(\pi N_2 h'_2)^2} \times \sum_m \sum_{m'} e^{-(\mu d/2)(m+m')[1/\sin(\theta-\omega) + 1/\sin(\theta+\omega)]} \times e^{-M(m)} e^{-M(m')} e^{2\pi i l (Z_m - Z_{m'})} e^{2\pi i (m-m') h_3}, \quad (3)$$

where μ is the linear absorption coefficient, d is taken as the average first-order interplanar spacing that locates planes m and m', and (hkl) planes are reindexed according to a $(00l)$ scheme. K' is constant over one intensity band, F is the structure factor for the normal unit cell, $N_1 a_1$ and $N_2 a_2$ are the dimensions of the crystal along a_1 and a_2 directions parallel to the free surface, and $h'_1 = (h_1 - h)$, $h'_2 = (h_2 - k)$, h_3 are variables in reciprocal space expressed in units of the reciprocal lattice vectors b_1, b_2, and b_3. The exponentials containing $M(m)$ and $M(m')$ are static attenuation factors [see Eqs. (7a) and (7b) in Ref. 4] which are discussed later. If $N_1 a_1$ and $N_2 a_2$ are taken to be large, the intensity in reciprocal space is spread only along the h_3 direction, and becomes a product of δ functions with respect to the h'_1 and h'_2 dependence. The variation of the intensity along the h_3 direction must be obtained by numerically summing Eq. (3) over the entire zone, assuming that the entire implanted zone diffracts coherently without interfaces. The displacement Z_m is obtained by summing to obtain the accumulated displacement along the 3 direction for each m position.

At this point, it should be pointed out that a d spacing profile was also obtained by approximating this curve by a system of connected linear elements.[4] We found that an almost identical profile could be obtained. The linear element model was not used in the final analysis because each element is taken to be incoherent with respect to all others. Incoherency can be achieved by the introduction of internal interfaces. However, this model implies that new interfaces are created. The latter is not considered to be an important occurrence and was abandoned in favor of a continuous coherent zone without internal boundaries.

Intensity band simulations based upon TRIM [Figs. 5(a) and 5(b) and Eq. (3)] are shown in Figs. 6(a)–6(d). Equation (1) of Ref. (4) was modified to include the absorption of the x-ray beam within a sample. The absorption of the x-ray beam within a surface layer of implanted zone thickness ~5000 Å is not significant for symmetrical beam optics, i.e., $\omega = 0°$, but it may have a considerable effect on the simulated profile when the tilt angle $\omega \approx 35°$. Because samples C1 and C2 have scattering contributions from a thick substrate, the direct summation of Eq. (4) is cumbersome to evaluate. In these cases, an analytical expression was used for the amplitude of scattering from the undisturbed substrate. This kinematic calculation takes absorption into account and the summation over the disturbed region is truncated when the d spacing reaches its unstrained value at ~5500 Å. The intensity contribution was divided into three parts: scattering from the disturbed implanted zone (evaluated numerically), cross terms between the implanted and unimplanted zones, and scattering from the undisturbed substrate. The last term gave a

[This article is copyrighted as indicated in the article. Reuse of AIP content is subject to the terms at: http://scitation.aip.org/termsconditions. Downloaded to] IP: 128.173.126.47 On: Wed, 06 May 2015 20:47:48

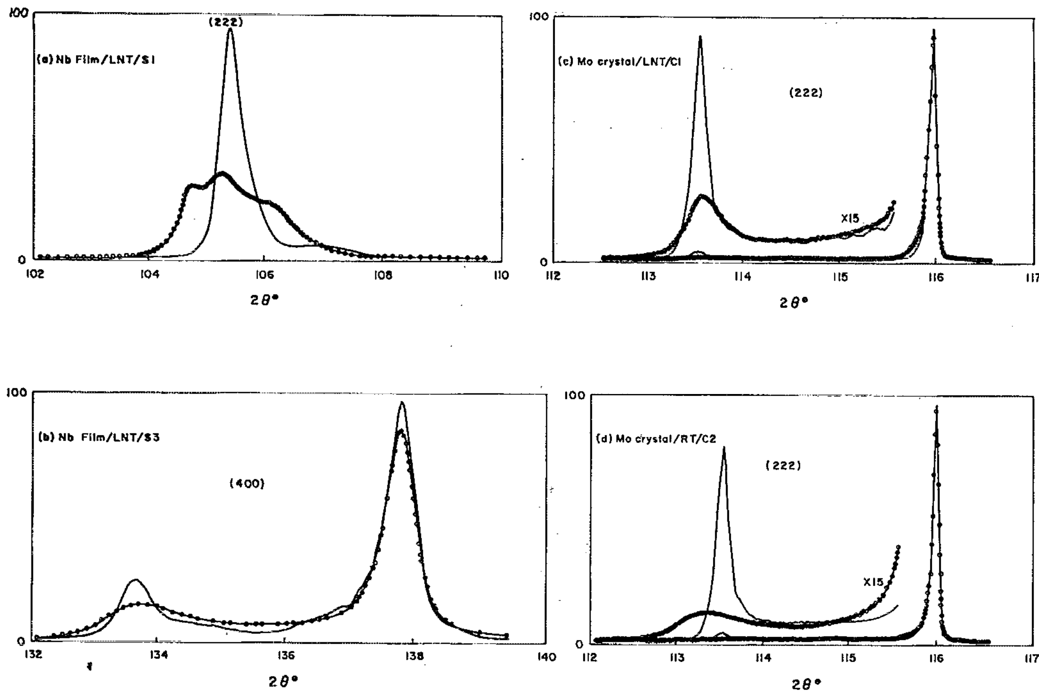

FIG. 6. Intensity band simulations for Nb and Mo using TRIM curves shown in Fig. 5.

very sharp peak at the unimplanted peak position with a total integrated intensity given by

$$I_s = \int I(h_3)dh_3$$

$$= \frac{Ke^{-\mu t_0[1/\sin(\theta_0-\omega)+1/\sin(\theta_0+\omega)]}}{\mu d[1/\sin(\theta_0-\omega)+1/\sin(\theta_0+\omega)]}, \quad (4)$$

where θ_0 is the unimplanted peak position, ω is the tilt angle, t_0 is the thickness of the implanted zone, μ is the linear absorption coefficient, d is the average d spacing and K is a constant for a given reflection. Cross terms were found to be insignificant so that the analysis for the present samples could have been carried out only by summing intensities from the implanted and unimplanted regions of the sample.

The calculated intensity profile includes a convolution with the profile measured from the unimplanted crystal film. This convolution provides a correction for instrumental broadening. The exponent of the attenuation factor M was calculated from the Green's function Kanzaki force method.[14] This provides the average static displacements required for M, which includes interstitial and loop sources.

A comparison between the theoretically simulated profiles and the experimental results [Figs. 6(a)–6(d)] does not give a good fit for all samples. The experimental and theoretical profiles have been scaled to an area of unity in comparing the shapes of the distributions. The fits using TRIM are poor with only the positions of the maximum in the diffraction profile in agreement. Therefore, the d spacing profile was refined by a trial and error procedure to fit the experimental intensity bands. The free expansion strain profiles that give the best fit to the intensity bands are shown in Figs. 5(a) and 5(b) and the corresponding fits are shown in Figs. 2(a)–2(d). The percentage misfit error varies between 4% and 8%. In the fitting procedure, the exponent of the attenuation factor M was taken to be linearly proportional to the strain along the X_3 direction, which is obtained from the d spacing profile as

$$\epsilon_{33}(X_3) = [d(X_3) - d_s]/d_s, \quad (5)$$

where d_s is the d spacing corresponding to the undisturbed substrate. The proportionality constant was varied to fit the average intensity attenuation from the implanted film as compared to the unimplanted film. In the case of Mo crystals, this was kept close to the value for N in Mo as obtained from Ref. 2, because experimental intensity ratios between implanted and unimplanted crystals could not be obtained with sufficient accuracy for our samples due to minor extinction effects. Although extinction was observed, intensities were within 20% of kinematic theory. The values of the proportionality constant $\alpha(dM/d\epsilon_{33})$, used in the fitting procedure, are given in Table III for the (222), (400), (220), and (321) reflections of Nb and the (222) and (220) reflections of Mo.

Experimental intensity profile data with angle $\omega \sim 35°$ are shown in Figs. 3(a)–3(d). The variation of ϵ_{33} with depth was obtained from a fit to the respective reflections at $\omega = 0°$ by projection. Both ϵ_{11} and ϵ_{22} are taken to be zero throughout the implanted crystal for the elastic model. $dM/d\epsilon_{33}$ and the absorption path lengths used in the fitting procedure depend upon (hkl). For these reflections, the absorption path lengths introduce significant reshaping of the intensity distributions. For the (220) reflection from Mo, with a tilt angle of 35.26°, the x-ray beam is attenuated 50% in an implanted zone of approximately $\sim$5000 Å. After projection along the radial direction, the simulated intensity profile was convoluted with the radial

[This article is copyrighted as indicated in the article. Reuse of AIP content is subject to the terms at: http://scitation.aip.org/termsconditions. Downloaded to] IP: 128.173.126.47 On: Wed, 06 May 2015 20:47:48

TABLE III. $\alpha = dM/d\epsilon_{33}$, at different reflections for implanted samples S1, S3, C1, and C2.

Sample	Reflection	$\alpha = dM/d\epsilon_{33}$
S1 (Nb, 111 film) implanted at LNT	222	20.41
	220	17.69
	321	28.57
S3 (Nb, 100 film) implanted at LNT	200	7.82
	400	29.73
	321	23.47
C1 (Mo, 111 crystal) implanted at LNT	222	15.76
	220	10.50
C2 (Mo, 111 crystal) implanted at RT	222	15.76
	220	11.20

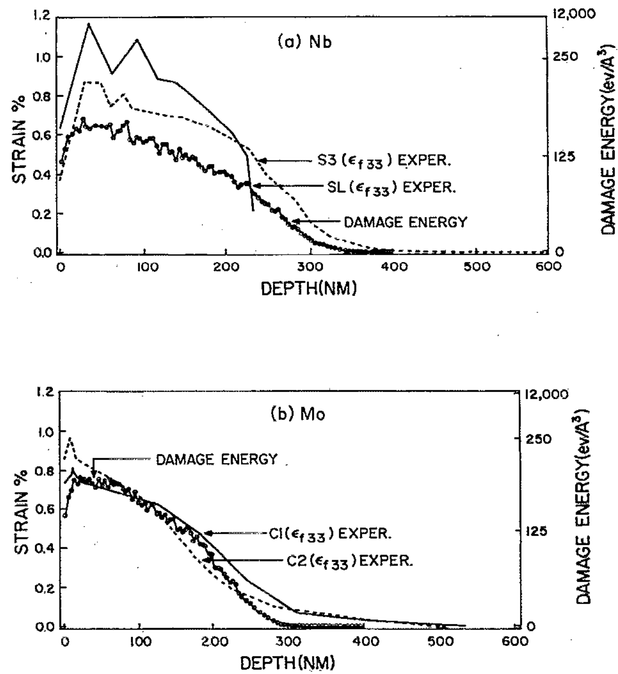

FIG. 7. Replots of free expansion strain (Fig. 5) with damage energy profile.

scan profile from the unimplanted film and then compared with the experimental data. This projection procedure, to evaluate the intensity profile for $\omega \neq 0°$ reflections, assumes that the implanted zone is in a state of pure elastic deformation. Figures 3(a)–3(d) show the fits to the experimental data. It is seen that the overall intensity profiles are predicted by the elastic model but the detailed fits are poorer with the Mo crystals.

Rocking curves were measured at five selected points, within an intensity band, from all the samples. Examples of rocking curves at various points along the (222) reflection from sample C1 are shown in Fig. 4. A 0.2° entrance slit was used to measure the rocking curve data. The Gaussian form for the rocking curves enables one to make use of a simple instrumental correction for the half-width,[5] i.e.,

$$\Delta\omega_c^2 = \Delta\omega_e^2 - \Delta\omega_i^2, \quad (6)$$

where the subscripts c, e, and i, refer to corrected, experimental, and instrumental half-widths. The rocking curves show a significant amount of broadening, increasing in regions where the d spacing profile shows the steepest gradient. This appears to be almost independent of the order of the reflection and is similar for all the implanted samples.

III. DISCUSSION

A comparison of the strain profiles that give the best fit to intensity band data from uninclined reflections ($\omega = 0°$) with TRIM predictions (Fig. 5) show that: (i) the strain profile close to the surface is larger than predicted, (ii) the strain profile shows some characteristic oscillations and fine structure near the surface in Nb films implanted at LNT, and (ii) the strain profile in the interior region ($\sim$1000–3000 Å from the surface) is smaller than predicted in all cases. The differences are larger in Mo crystals than in Nb films. In an effort to understand these differences, the spatial distribution of knock-on energy damage for the four-step implantation process was simulated using an extended version of TRIM.[15] Figure 7 shows the results of this simulation along with the strain profiles obtained by x-ray diffraction. In all cases, the shape of the experimental strain profile approaches the shape of the corresponding damage energy distribution. This suggests that N implants diffuse preferentially towards regions of high damage energy. The four N implantations were carried out sequentially in order of decreasing energy, causing the damage energy distribution for each successive implantation to be shifted closer to the free surface. This causes N atoms already in a crystal to undergo enhanced diffusion towards the surface. The corresponding profiles from Mo crystals C1 and C2 appears to be more greatly affected than the Nb data (See Fig. 5). This is in agreement with the simulated energy deposition curves for Mo and Nb. The difference between Mo and Nb energy deposition curves is due largely to the higher atomic density of Mo ($\approx$15%).

A calculation of the average amount of N in Mo, derived from the experimental strain profiles of Fig. 2(b), shows that it is $\sim$25%–30% smaller than what is predicted from TRIM. This is true at both LNT and RT, and may be due to the trapping of N at knock-on-damage-produced defects, like vacancies. The lattice parameter data from N-implanted polycrystalline Mo films[2] was explained in terms of N vacancy pairing in Ref. 16. It was estimated that approximately 50% of the single N interstitials were trapped at vacancies after implantation into a polycrystalline Mo film using similar fluences. The present data on single crystals C1 and C2, can be explained in terms of trapping of 25%–30% of the implanted N interstitials at vacancies. The differences between the data on single crystals and polycrystalline Mo films may be due to the presence of additional relaxation mechanisms found in polycrystalline films. Grain-boundary and dislocation densities are larger in polycrystalline Mo films. Such mechanisms for the relaxation of internal stress fields around N

[This article is copyrighted as indicated in the article. Reuse of AIP content is subject to the terms at: http://scitation.aip.org/termsconditions. Downloaded to] IP: 128.173.126.47 On: Wed, 06 May 2015 20:47:48

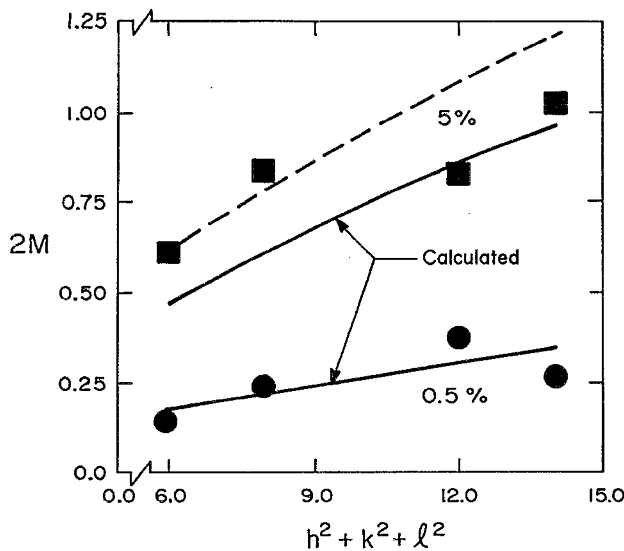

FIG. 8. $2M$ factors for N-implanted Nb at LNT. Squares are from 5-at. % (S1) and circles are from 0.5-at. % samples. Solid curves are calculated for each concentration level. The dashed line is an estimate of $2M$ for di-interstitials at 5 at. %.

implants in Mo single crystals are less likely. Calculations for Nb films did not show a similar relaxation effect.

Initially, it was believed that the fast falloff of the d spacing profile in the interior of the implanted Nb film (S1) is due to the presence of mixing at the Nb-sapphire interface. However, a careful examination of the sapphire substrate reflection (012) indicated that there is no observable change in the shape of this peak. Therefore, there is no evidence to support penetration of implanted N or for damage of the underlying substrate lattice. A small amorphous region at the interface could go undetected.

To summarize, the strain profile of sample S1 shows a larger than expected decrease close to the interface (~ 100 Å from the interface), and a compensating increase closer to the surface. For Mo samples, there is evidence for significant channeling of N implants into the Mo lattice at depths >3000 Å. That is, the experimental strain profiles tend to extend more deeply than predicted by TRIM.

Static exponential attenuation factors (2M) from four Bragg peaks were obtained by taking a ratio of the integrated intensity from an implanted Nb sample to an identical one which was not implanted. This procedure also served to cancel the corresponding thermal factor. Experimental values for Nb implanted at LNT are shown as points in Fig. 8 with squares representing 5 at. % and circles the 0.5-at. % sample. Each of the solid curves are calculated for N located as single interstitials in octahedral positions and loop distributions given in Ref. 17. That is, the same loop distributions were taken at 5- and 0.5-at. % levels. This assumes that saturation has occurred at or below 0.5 at. %. With 0.5-at. % N and energies given in Table I, one finds that each atom undergoes six major displacements that should provide a safe lower level for saturation. The dashed curve is an estimate for N present as di-interstitials at the 5-at. % level. From these results at LNT, one cannot rule out the possibility of a mix of single, di-interstitials and possibly a small fraction of tri-interstitials at the 5-at. % N level. Diffuse scattering data suggests that at 0.5 at. % there is a dominance of single interstitials.

Attenuation factor data from a Nb film implanted with N to a level of 0.5 at. % at room temperature has been found to be approximately a factor of 2 larger than the values obtained for the film implanted to 0.5 at. % N at LNT. If it is assumed that the total number of point defects (interstitials and vacancies) retained in RT-implanted film is identical to the number in the LNT-implanted film and that they are located in $(211)[11\bar{1}]$-type loops, we find that both vacancy and interstitials loops are twice as large in the RT-implanted film as compared with the LNT implanted film. This is based upon the finding that the attenuation factor per unit point defect for a loop scales approximately as its radius.[18]

We have used the elastic model in comparing the d spacing profile obtained from experimental data with TRIM calculations, i.e., the sample is assumed to provide a container with rigid walls. Therefore, the implanted zone is only allowed to expand elastically perpendicular to the free surface.[7] Such a model can be verified by analyzing intensity distributions from planes inclined to the surface of the implanted zone. An ideal elastic model requires the normal strain at angle ω to the surface normal ϵ_ω to be related to the surface normal strain, ϵ_{33}, according to

$$\epsilon_\omega = \epsilon_{33} \cos^2\omega. \quad (7)$$

At an angle $\omega \sim 35°$, the strain gradient $\epsilon_\omega(z)$ is only 60% of the strain gradient $\epsilon_{33}(z)$. If the substrate is not rigid and there is complete relief of the elastic stresses, the strain data are independent of tilt angle and $\epsilon_\omega(z) = \epsilon_{33}(z)$.[7] Equation (7) hold for all samples that are under investigation. The small differences that are observed are due to experimental or instrumental effects.

Rocking curves from various depths within the implanted zone display a small but measurable broadening that is not predicted from an ideal elastic model [see Figs. 4(a)–4(e)]. Also, some misfit is observed at the extremes at the intensity bands obtained from planes inclined ($\sim 35°$) from the free surface. An ideal elastic model should give an equally good fit for all intensity bands. We believe that both effects are due to small amounts of lattice bending in regions of highest stress. Some localized kinking or bending could selectively influence the widths of both the rocking curves and 2θ scans. This effect is likely to originate from only a small fraction of the overall volume of an implanted zone in a way that allows the overall zone to remain elastic with very little plastic deformation.

In order to arrive at unique d spacing profiles, absorption must play a significant role over implantation distances. If this distance is too small the top of the zone cannot be distinguished from the bottom. For the (222) intensity band, using Mo and Nb with CuKαl radiation, there is only a 5% difference in beam absorption over 2500 Å. When the (220) intensity band is examined at $\omega \sim 35°$, beam absorption introduces a 40% correction for the same depth. Under these conditions rotating the d spacing pro-

[This article is copyrighted as indicated in the article. Reuse of AIP content is subject to the terms at: http://scitation.aip.org/termsconditions. Downloaded to] IP: 128.173.126.47 On: Wed, 06 May 2015 20:47:48

files 180° so that the free surface becomes substrate would give obvious misfits when the intensity bands are simulated.

IV. CONCLUSIONS

The following conclusions are based collectively upon three different x-ray measurements. These include exponential attenuation factors ($2M$), diffuse x-ray scattering, and d spacing profiles. These measurements and analyses are described in this paper or in a preceding one.[17] All require a knowledge of the displacement fields and related changes in the lattice parameters. The major elastic field disturbance, based upon previously documented evidence, is due to N located in octahedral sites.[1] Di- and tri-interstitials are likely to be present in the 5% Nb sample implanted at LNT. Our findings do not exclude the presence of more complex interactions between defects. Rather, the picture presented here should be considered as the simplest model that fits all three forms of data. In the case of Mo samples only d spacing profile data has been reported here. These data suggest that the similarities between the behavior of Nb and Mo are stronger than their differences which are given below. To summarize, the following have been concluded.

(i) With ~ 5 at. % of N implanted at LNT into Nb, our calculations indicate that the dominant elastic residual strain arises from volume changes associated with single N interstitials located in octahedral sites. Defects produced by radiation damage are in the form of small vacancy and interstitial loops which produce residual strains of minor importance. This originates almost entirely from their core regions which give a positive expansion. Most of the potential contribution to the residual long-range strain cancels due to equal and opposite volume changes from vacancy and interstitial loops. However, local nonuniform fields are present and have an effect on intensity measurements through the $2M$ factor.

(ii) The behavior of the Nb 2500-Å with a sapphire interface is different than the thicker 6000-Å film. Here the N prefers to remain in the thinner Nb film forming a somewhat larger gradient. This behavior is probably related to the highest-energy implantation where the Gaussian-like TRIM distribution would extend beyond the Nb-sapphire interface if the Nb film were thicker. Clearly, the 6000-Å (100) film gives the best agreement with TRIM and provides a better comparison due to its greater thickness.

(iii) Mo single crystals implanted to ~ 5 at. % N show a more complex behavior. There is an apparent loss of expansion centers associated with single N interstitials in octahedral sites for both LNT and RT implantations. This may be due to the following: N vacancy complexes, N association with dislocations or sub-boundaries, or to a lesser extent N loss at the free surface.

(iv) For both Nb and Mo, the original N distributions become shifted toward regions of high knock-on energy depositions. This shift is believed to arise from enhanced diffusion and is most pronounced for Mo samples. The redistribution is found to be larger in the RT-implanted sample than from one implanted at LNT.

(v) Both Nb and Mo substrate lattices behave like rigid containers in directions parallel to the free surface. This gives a magnified elastic displacement normal to the free surface. Kinking or bending in regions of highest strain gradient could be presented as a small fraction of the sample volume.

ACKNOWLEDGMENT

We would like to acknowledge the Office of Naval Research for sponsoring this research on Grant Number N0004-83-K-0750, P00004.

[1] H. Dosch and J. Peisl, Phys. Rev. B **32**, 623 (1985).
[2] G. Linker, Nucl. Instrum. Methods **182/183**, 501 (1981).
[3] V. Schubert, H. Metzger, and J. Peisl, J. Phys. F. **14**, 2457 (1984).
[4] S. I. Rao and C. R. Houska, J. Appl. Phys. **69**, 8096 (1991).
[5] C. R. Houska, in *Treatise on Materials Science and Technology, Experimental Methods*, edited by H. Herman (Academic, New York, 1980), Vol. 19A, p. 63.
[6] C. R. Houska, J. Appl. Phys. **41**, 69 (1970).
[7] S. I. Rao and C. R. Houska, J. Mater. Sci. **25**, 2822 (1990).
[8] S. I. Rao, K. Grabowski, C. R. Houska, G. Ice, and A. Habenschus, in Materials Research Society Symposia Proceedings, Fall Meeting, 1988.
[9] J. S. Vermaak and J. H. Van Der Merwe, Philos. Mag. **10**, 875 (1964).
[10] P. G. Winchell, J. Boah, and P. S. Ayers, J. Appl. Phys. **42**, 2612 (1971).
[11] TRIM, a Monte Carlo Computer Code Used to Simulate the Distribution of Implants and Energy Deposition, Naval Research Laboratory, Washington, DC.
[12] B. He, S. I. Rao and C. R. Houska, J. Mater. Sci. **25**, 2667 (1990).
[13] G. Simmons and H. Wang, *Single Crystal Elastic Constants and Aggregate Properties: A Handbook* (MIT Press, Cambridge, 1971).
[14] S. I. Rao, E. J. Savino, and C. R. Houska, in "Characterization of Defects in Materials," Mat. Res. Soc. Symp. Proc., Vol. 82, p. 187 (1987). Ed. R. W. Siegel, R. Sinclair, and J. R. Weertman.
[15] D. Farkas (personal communication and unpublished simulations).
[16] S. I. Rao, K. Grabowski, and C. R. Houska, Nucl. Instrum. Methods B **27**, 296 (1984); B **27**, 396 (1987).
[17] S. I. Rao, C. R. Houska, K. Grabowski, G. Ice, and C. Sparks, J. Appl. Phys. companion paper.
[18] P. H. Diederichs, Phys. Rev. B **4**, 1041 (1971).

[This article is copyrighted as indicated in the article. Reuse of AIP content is subject to the terms at: http://scitation.aip.org/termsconditions. Downloaded to] IP: 128.173.126.47 On: Wed, 06 May 2015 20:47:48